J Nondestruct Eval (2015) 34:16
DOI 10.1007/s10921-015-0288-6

Determination of Magnetisation Conditions in a Double-Core Barkhausen Noise Measurement Set-up

Marek Augustyniak[1,2] · **Bolesław Augustyniak**[1] · **Leszek Piotrowski**[1] · **Marek Chmielewski**[1]

Received: 24 February 2015 / Accepted: 2 May 2015 / Published online: 2 June 2015

Abstract The magnetic Barkhausen effect is useful for assessing 1D and 2D stress states of ferromagnetic steel objects. However, its extension to technically important materials, such as duplex anisotropic steels, remains challenging. The determination of magnetisation inside the studied object and the electromagnet for various geometries, materials and magnetisation angles is a key issue. Three-dimensional, dynamic finite element analysis has been applied to reproduce time-varying fields inside and outside the prototype of a double-core magnetising setup. Useful relationships between characteristics (peak height and location) and magnetic induction vector have been proposed. The qualitative plausibility of simulation has been validated with an experiment and an analytic formula of skin depth. The angular anisotropy of magnetic Barkhausen effect (MBN) in an isotropic sample has been shown in simulation and confirmed experimentally. The numerical model, despite some limitations, seems to be an efficient tool for calibrating stress/MBN relationships at least in isotropic structural steel components.

Keywords Electromagnetic finite element method · Dynamic magnetisation of bulk volume · Eddy currents · Magnetic Barkhausen effect (MBN)

✉ Marek Augustyniak
maugustyniak@mif.pg.gda.pl

[1] Gdansk University of Technology, 80-233 Gdansk, Poland

[2] DES ART Ltd., 81-969 Gdynia, Poland

1 Introduction

Deducing surface stress state of the ferromagnetic steel structures is one of the most significant goals of the NDT community. The Barkhausen effect has been applied in this context for more than two decades [1–3]. Its applicability is easy to demonstrate in simple laboratory set-ups, where controlled uniaxial stress change causes significant monotonic variations of magnetic Barkhausen effect (MBN) [4]. Effect of biaxial stress has been intensively studied as well [5,6], and procedures exist to determine principal stresses from orthogonal MBN measurements, as long as a given steel grade has been properly calibrated in advance.

As in any NDT technique, the inverse, in-situ problem remains a challenge, for several reasons. Firstly, the magnetic field distribution and its time variation within the material cannot be measured directly, so there can be doubts about the repeatability and controllability of the measurements. Because of the trade-off between measurement speed and accuracy, the choice of optimal frequency, amplitude [7] and number of sampled points / probe angles remains open. Secondly, even if the field was well-defined, some uncertainties would remain as to the fundamental sources of MBN. Can its main characteristics (peak location, height and width) be derived from B, dB/dt? Thirdly, the material data, both magnetic and structural, are subject to uncertainty and variation with heat treatment and degradation [3,8]. Finally, there are technically important materials, like duplex steels, which exhibit very significant magnetic anisotropy. Although some work has been started [9], detailed stress assessment procedure is still missing.

The Authors of this paper have mainly dealt with the first and the second issue, using Finite Element modelling strategy which has proven useful and reliable in our previous works [10,11].

Although the application of a nonlinear transient magnetic FEA in the context of MBN-based NDT is our original, unique contribution, the concept of a double-core measurement set-up is not new. It has first been suggested and implemented by Vengrinovic and Tsukerman in 2004 [12], and used to produce co-called directional diagrams (DD), demonstrating significant sensitivity on plane stress state and texture of the tested material.

The magnetisation time- and space characteristics obtained by numerical simulation can provide an input to a feedback control system, thus allowing it to achieve arbitrary shapes and amplitudes of magnetic field waveforms inside the tested structure. The discussion of types and possible enhancements of feedback methods in magnetic circuits can be found in works by Zurek et al., Polik and Kuczman as well as White et al. [13–15].

Several abbreviations have been introduced in the article:

BSUM resultant magnetic induction—most important output from the finite element analysis; calculated as square root of sum of squares of B_x, B_y and B_z components at a specified location, usually central point

CP Central Point—critical location in the geometric centre of the magnetised area, where a ferrite MBN probe is placed

CAx Central Axis—the vertical axis of symmetry of the Set-up, including CP

DCMS double-core magnetising set-up—a prototype with four coils wrapped on two perpendicular C-cores (further referred to as X-Core, Y-Core). The applied sinusoidal excitation currents agree in phase, but may have different amplitudes.

AX, AY Amplitudes of source current densities on X-Core and Y-Core, expressed in MA/m^2

SCM source current magnitude—useful convention for describing the excitation strength. Calculated as square root of sum of squares of AX and AY

AMA actual magnetisation angle—derived from calculated results and/or Hall-probe measurements - represents the real induction vector orientation at the central point.

NMA nominal magnetisation angle—directly derivable from AX and AY, defined as arctan (AY/AX); in trivial cases, such as AY = 0, NMA = AMA, due to perfect symmetry

2 Model Description

2.1 Finite Element Mesh

A series of finite element simulations has been performed in ANSYS software with electromagnetic functionality. The dimensions of main components, namely X-core, Y-core and the plate have been taken from experimental prototype. The 20-node elements with edge-flux formulation have been applied. Hexahedral, refined discretisation has been defined within the plate and the cores, while the surrounding air space is filled with tetrahedral, relatively coarse elements. There is a gradient of edge length along the plate's depth, with thinnest elements (0.4 mm) at the top surface, and maximum thickness of about 1 mm at the bottom. Dirichlet (flux-parallel) boundary conditions were applied to all the walls of the 6-sided hexahedral model space (Figs. 1, 2).

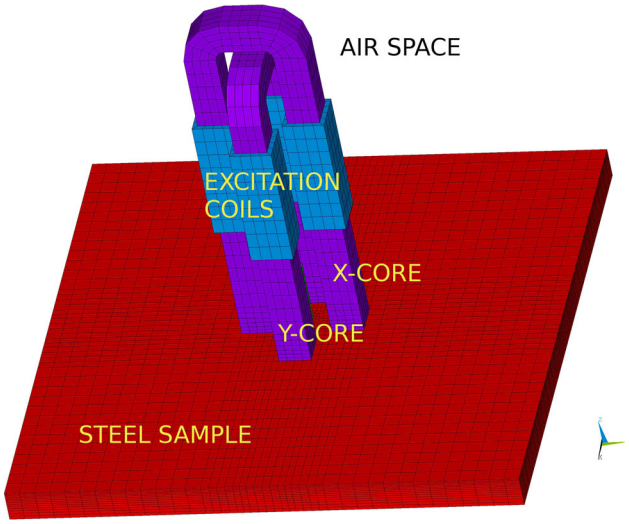

Fig. 1 General view of the FE model

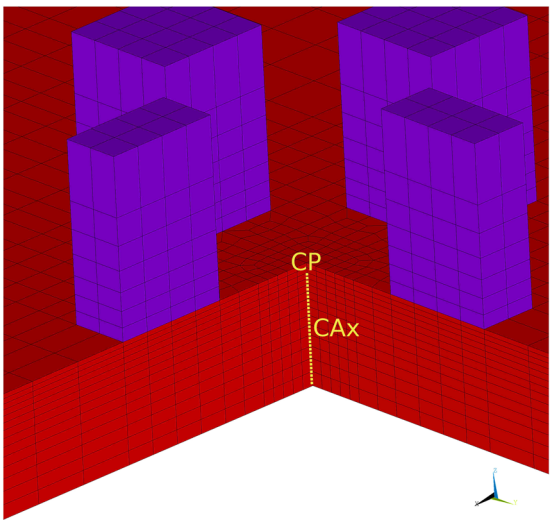

Fig. 2 Location of the central point (CP) and the central axis (CAx)

2.2 Material Model

The steel has constant electrical conductivity of 5 MS/m. The cores are perfectly laminated, i.e. they do not exhibit any eddy

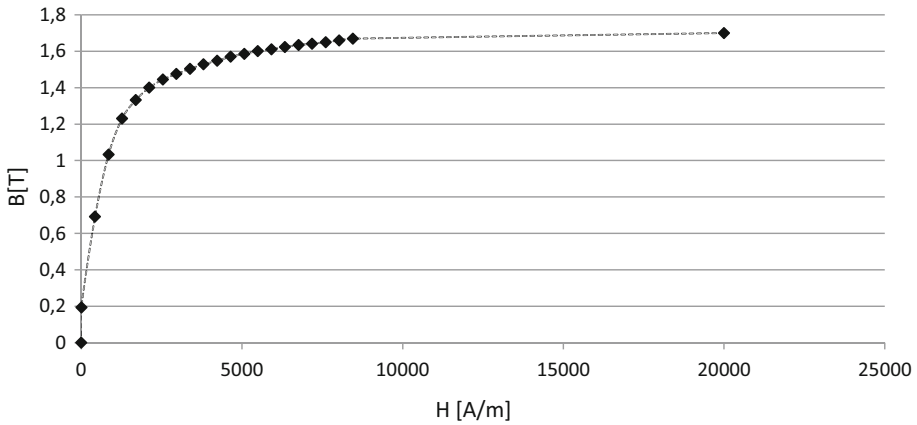

Fig. 3 B(H) *curve* of the magnetised plate (EN P255 steel grade)

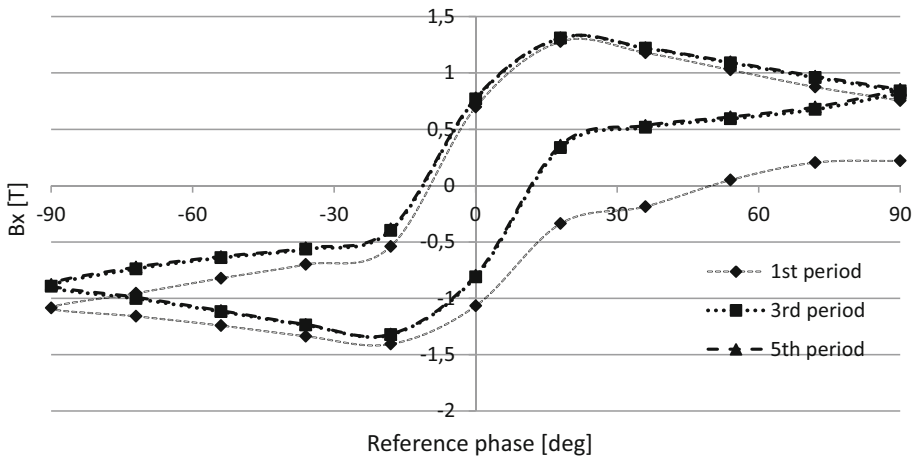

Fig. 4 Solution stability check; time-variation of the "x" component of magnetic induction at CP, in three selected periods of the excitation cycle (NMA = 0); reference phase of 0° corresponds to zero excitation current;

current effects. The surrounding air has zero conductivity and relative magnetic permeability of 1.0. The steel plate has been given B(H) nonlinear curve as plotted on Fig. 3, which was found to be representative for large family of low-carbon steels. The cores have got a nonlinear B(H) characteristic as well, based on pure-iron properties (saturation induction of ca 1.7 T).

2.3 Solution Scheme and Stability Check

The simulation is transient, and the magnetic induction distribution results from time-varying current density loading on four excitation coils. The amplitudes of current densities (max. of 0.8 MA/m^2) are based on the preliminary setting of the prototype. Two coils wound on a common core work in series, i.e. they have got identical electromotive forces (EMFs) which add up. The X-core and Y-core loadings are controlled independently, but there is no phase shift between them, i.e. the zero-current and maximum-current occurs at the same instant.

A convention of phase shifts "φ" was adopted, according to which the zero-current corresponds to $\varphi = 0$, minimum-current to $\varphi = -90$ and maximum current to $\varphi = +90$. The variation of magnetic induction may be thus related to this reference angle.

During test runs, the convergence of the Newton-Raphson scheme was invariably poor at the first time-step. Success was achieved only when an extra static step was introduced, the allowable number of substeps was increased and the tolerance of solution error was temporarily loosened. Nevertheless, high magnetic permeabilities of order of 50,000 (corresponding e.g. to permalloy cores) still produced convergence failure.

The solution stability was another issue on which results accuracy depended (see Fig. 4). The second calculated period differed significantly from the first one, so the results had to be treated as numerical, unrealistic transients. The 3rd, 4th and 5th period turned out to be similar to the second one and could be treated as a stabilised enough, reliable solution.

The applied software ANSYS has no intrinsic B–H hysteresis feature, but it can represent eddy-current, 'apparent' hysteresis. This notion can be defined as a hysteretic dependency between the source excitation current and the magnetic induction within the magnetised object. The carbon steels typically exhibit intrinsic hysteresis of order of 100 A/m. The eddy-current, apparent coercivity H_{ce} obtained from the

simulation at 10 Hz was of order of 500 A/m. This value has been derived from the phase shift between the zero-crossings of source current and the magnetic induction, related to 90° and multiplied by maximum value of magnetic field intensity, H_{max}.

3 Results

3.1 Contour Plots at Zero and Maximum Excitation Currents

Figures 5 and 6 show the zero-current/max.-current phases respectively, in case of Nominal Magnetisation Angle (NMA) equal to 60°. The source current magnitude (SCM) is set to 6 MA/m^2 which is of the order of magnitude of experimental current amplitudes. The instant of zero-SCM (Fig. 5) does not coincide with close-to-zero magnetic inductions, because eddy currents introduce some inertial effects and striking "turn-around" of flux lines within the central zone of the plate. The current-max. phase produces more uniform induction distribution, however it is surprisingly symmetrical with respect to the 45° line, although the ratio of current amplitudes AY:AX ∼7:4. The induction in bottom segments of the cores differs in proportion 5:4, and the induction components BY,BX at the central point (CP) remain almost equal.

Figures 7 and 8 show the BSUM induction distribution in the topmost layer of the plate for NMA = 0°, at $\varphi = 0$ (zero excitation) and 90° (maximum excitation) respectively. The Y-core disturbs the field distribution even though its coils are unloaded all the time. It is argued, that the laminated core material leads to local decrease of flux density, providing an extra low-reluctance pathway for flux lines. Again it is interesting to note, that at zero-current phase, the induction values are far from being negligible, e.g. there are regions of B>1.0T.

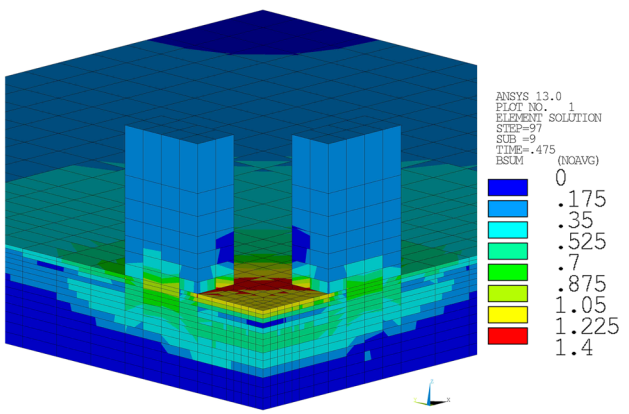

Fig. 5 Magnetic induction magnitude (BSUM) at instant of zero magnetising current; nominal magnetisation angle equal to 60°

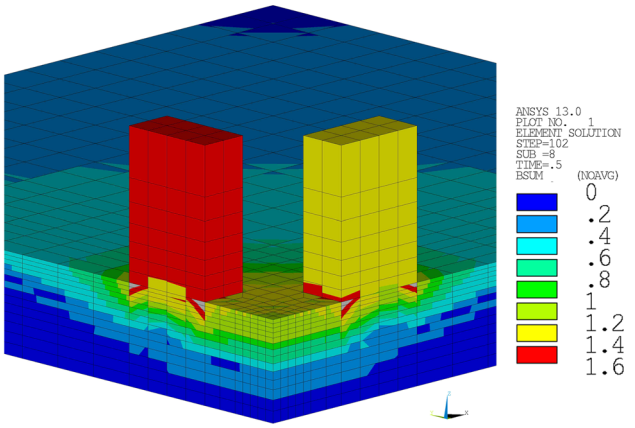

Fig. 6 Magnetic induction magnitude (BSUM) at instant of maximum magnetisation current (SCM = 6 MA/m^2); nominal magnetisation angle equal to 60°

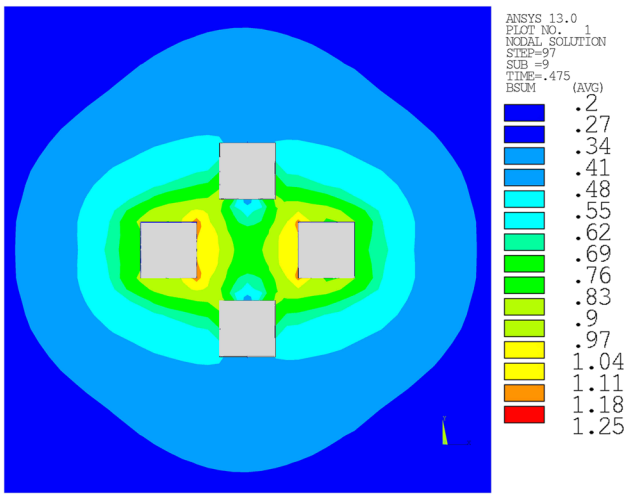

Fig. 7 Magnetic induction magnitude (BSUM) at instant of zero magnetising current; nominal magnetisation angle equal to 0°

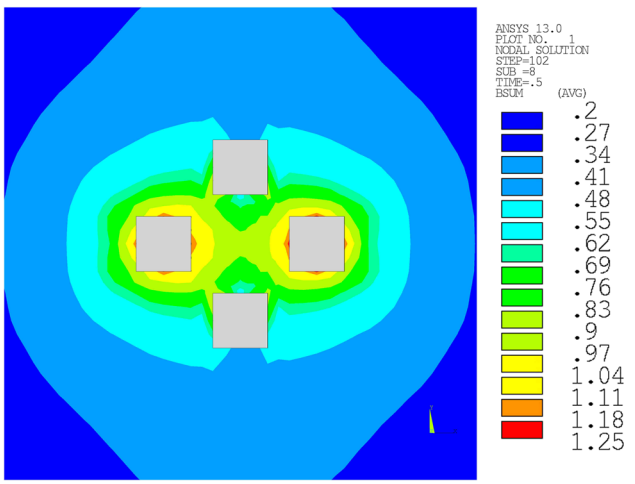

Fig. 8 Magnetic induction magnitude (BSUM) at instant of maximum magnetisation current (SCM = 6 MA/m^2), nominal magnetisation angle equal to 0°

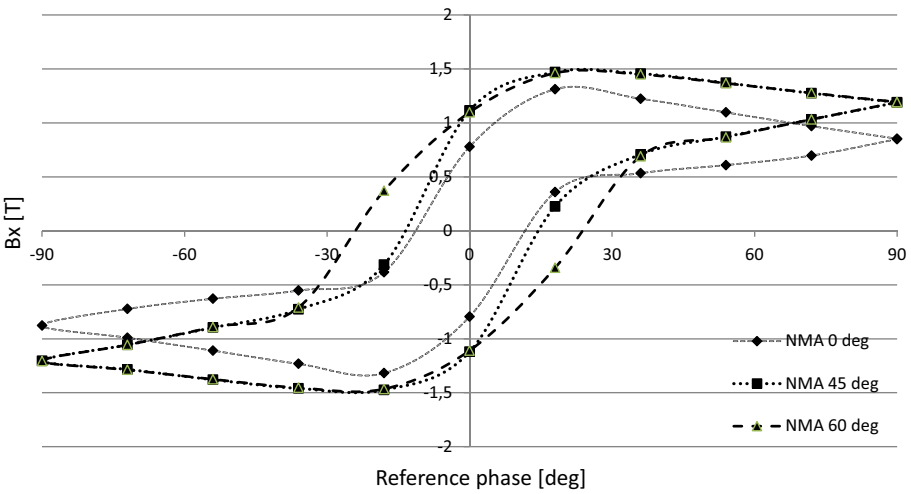

Fig. 9 Time-variation of magnetic induction at Central Point, for nominal magnetisation angle (NMA) equal 0°, 45° and 60°; reference phase of 0° corresponds to zero excitation current

3.2 Analysis of Time-Variation of Magnetic Induction Along the Central Axis (CAx)

The magnetic field time-dependency does not vary with angle when the single core is being mechanically located at different angles. Experience with DCMS prototype shows however some variations of MBN as a function of Nominal Magnetisation Angle. Plot 9 demonstrates calculated time-dependencies of signed magnetic induction magnitude at the Central Point. Three Nominal Magnetisation Angles (NMA), namely 0°, 45° and 60° are considered. The Source Current Magnitude (SCM) is kept constant at 6 MA/m^2 (Fig. 9).

Three characteristic values for each curve are compared. The zero crossing phase amounts to about 12°, 15°, and 24° for Nominal Magnetisation Angle (NMA) of 0°, 45° and 60° respectively.

The maximum B reaches 1.3, 1.5, and 1.5 T (0°/ 45°/ 60°).

The maximum B change rate dB/dt is calculated as 232, 286, 216 T/s (0°/ 45°/ 60°).

Simulation shows that it is harder to magnetise the sample at 0° than at 45° or 60°. The effect may be accounted for by the saturation/nonlinearity of the core, which is the most significant when a single core is loaded with the entire RSC, i.e. at 0°.

Actual Magnetisation Angles (AMA) are calculated as 0°, 46°, and 48°, for Nominal Magnetisation Angles of 0°, 45° and 60°, respectively. The surprising discrepancy between AMA and NMA at 60° may again be associated with the saturation effects. The core which is more intensely loaded saturates more significantly, so larger proportion of its flux is lost in form of stray fields, and the flux within the circuit is reduced due to lower effective magnetic permeability. Consequently the flux values penetrating the sample from both cores become closer. This results in BX/BY ratio at the Central Point (CP) tending to 1.0, and Actual Magnetisation Angle (AMA) approaching 45°.

Although the first top layer generates most of the MBN, it is useful to study the B time-through-depth dependency. Activity of eddy currents within the deeper layers entails retardation of magnetic induction with regard to the source current. This phenomenon is termed as "eddy-current hysteresis". The conservation of Gauss theorem requires that the sum of fluxes in all the layers be approximately proportional to the source currents. In particular, the total flux must zero-out at $\varphi = 0$. Consequently, the surface layers exhibit field of opposite sign, appearing as "advanced in phase" (Fig. 10).

Analysis of the numerical data behind Fig. 10 indicates a non-trivial phenomenon of hysteresis loop reversal between surface (1) and deeper (especially 7+) layers. The intermediate (4th) layer exhibits unusual hysteresis loop with two self-crossings.

3.3 Through-Depth Field Decay

The distribution of magnetic flux inside a ferromagnetic bulk sample depends significantly on the source current frequency. The well-known skin-depth formula (1) has been found to be relevant in similar set-up [16], so it can be reapplied in the double-core set-up.

$$d = \sqrt{\frac{2}{\omega \mu_r \mu_0 \sigma}} \tag{1}$$

where

- ω – angular frequency
- μ_r – relative magnetic permeability (dependent on local H)
- μ_0 – absolute magnetic permeability of the vacuum
- σ – electrical conductivity of the sample

The skin-depth "d" corresponds to the distance from the surface at which the induction amplitude decreases by the factor of 2.71 ("e").

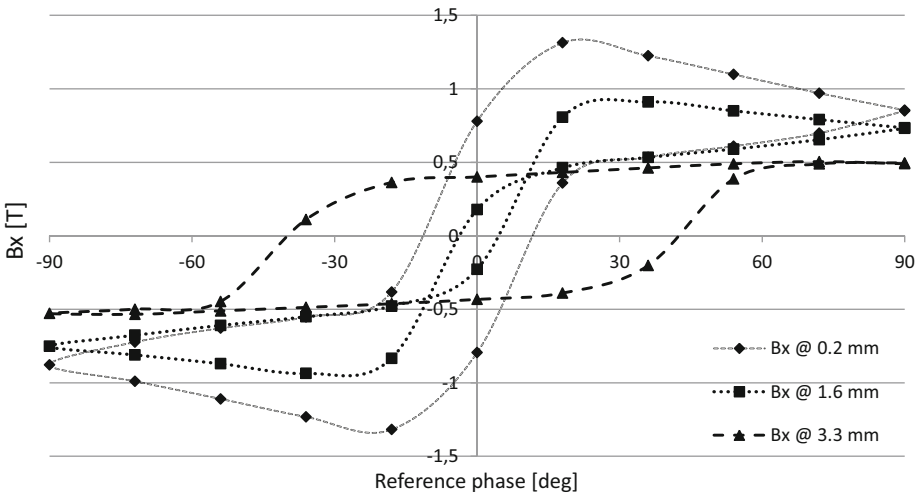

Fig. 10 Time-variation of magnetic induction at various depths from the plate's *top* surface; nominal magnetisation angle (NMA) equal to 0°; source current magnitude equal to 6 MA/m^2

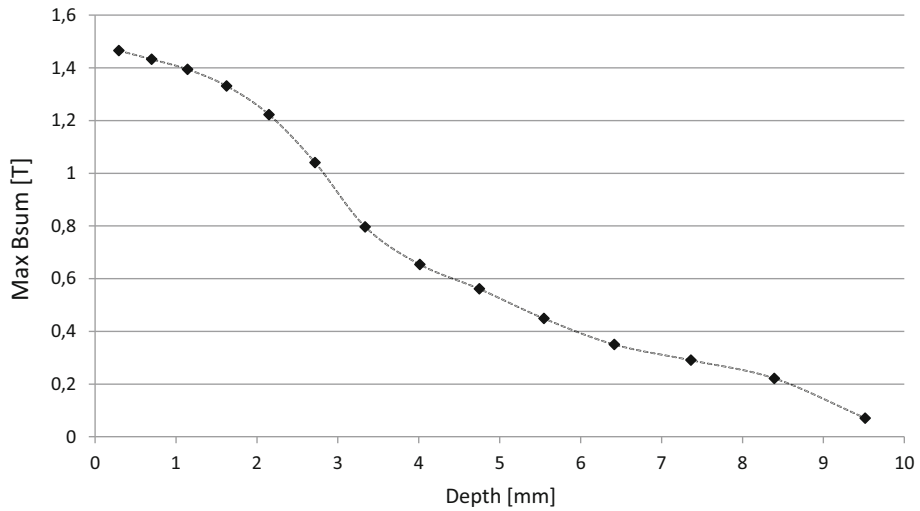

Fig. 11 Maximum value of BSUM at various depths from the plate's *top* surface

It is expected, that the magnetic induction B reaches highest values at the surface, and its amplitude (maximum value in time) decreases with depth. The simulation run at nominal 60° with relatively "high" source currents (source current amplitude of 6 MA/m^2) has been selected to examine the through-depth induction variation and compare it against analytical formula.

The assumed B(H) curve leads to varying estimates of d as a function of local H. At H = 100, 1000 and 5000 A/m, d∼2, 6, 15 mm respectively.

The calculated induction amplitudes at varying depths are shown in Fig. 11. The decrease by factor ∼3 at 6 mm correlates well with the analytical prediction.

3.4 Comparison of Low-Current Versus High-Current Magnetisation

Two series including the total of 6 simulations have been performed. Three of these had the elevated source current magnitudes (SCM) of 6 MA/m^2, three others had the SCM of 0.3 MA/m^2. In both series the nominal magnetisation angle (NMA) was set to 0°, 45° and 60°. The induction magnitude (BSUM) was recorded at the Central Point as a function of the phase of the magnetising current. The comparison at 60°, for high SCM versus low SCM is shown in Fig. 12.

The low magnetising currents allow operating within the linear portion of the B(H) curve, producing induction magnitudes not exceeding 0.6 T, whereas the selected high SCM causes a very prominent non-linearity due to saturation of the cores and the central area of the plate, with BSUM approaching 2 T. In such a case, the time-variation of any component of the induction is no longer monotonic when the magnetising current increases from its negative peak value up to the positive peak value. This strong non-linearity and lack of monotonic behaviour make the setting unsuitable for interpretable Barkhausen Noise measurement.

The comparison of nominal magnetisation angle (NMA) and actual magnetisation angle (AMA) is shown in Table 1. The difference is negligible at NMA = 0°, regardless the SCM. At 45° the discrepancy, due to the inequality of

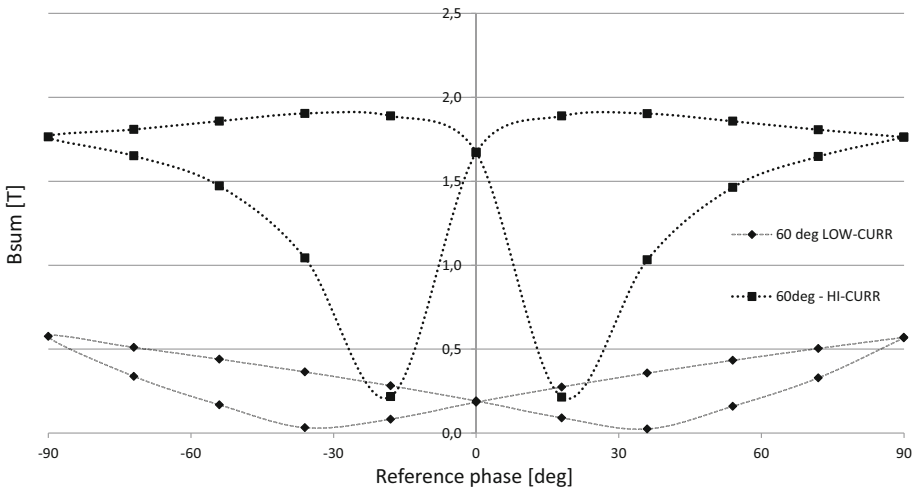

Fig. 12 Time-variation of magnetic induction magnitude BSUM at low current (3×10^5 A/m^2) and high current (6×10^6 A/m^2), at the central point of the plate's top surface; nominal magnetisation angle (NMA) equal to 60°

Table 1 The comparison of nominal magnetisation angle (NMA) and actual magnetisation angle (AMA) for three NMAs and low/high source current magnitude

Nominal magnetisation angle (NMA)	Actual magnetisation angle (AMA) High source current of 6×10^6 A/m^2	Actual magnetisation angle (AMA) Low source current of 3×10^5 A/m^2
0°	0°	0°
45°	46°	42°
60°	49°	57°

lengths of the C-Cores, does not exceed 3°, and still can be deemed negligible in practice. However, a significant difference between NMA and AMA (11°) is observed for NMA = 60°, and high source current Magnitude. The induction vector at the central point deviates from expected 60° towards the 45° direction. It is argued, that one of the C-Cores penetrates deeper into the magnetic saturation region. As its differential magnetic reluctance increases, it generates more stray field, which does not enter the plate. Consequently, uneven saturation of the C-Cores leads to a decrease of difference between BX and BY at the Central Point of the plate. This, in turn, results in AMA approaching 45°. Unequal air gaps at the poles in the actual system (e.g. operating over a curved surface) may play some role too, calling for an application of some flux control system, in order to balance the flux contributions from both cores.

4 Summary and Perspectives

A practically useful, 3D nonlinear dynamic Finite Element model of the double-core Barkhausen noise (DCBN) measuring setup has been constructed. The convergence of calculations has been achieved for the default operational frequency of 10 Hz.

Original definitions (NMA—nominal magnetisation angle, AMA—actual magnetisation angle, SCM—source current magnitude) have been proposed for the sake of unambiguous characterisation and repeatability of measuring conditions.

Insight has been obtained into the time/space distribution of the magnetic induction within the studied plate as well as the C-Cores, which is essential for planning and interpreting any magnetic-field based NDT procedure. The following observations have been made:

- The eddy current-related hysteresis loop is strongly dependent on the depth of the plate at which it is recorded. It exhibits a characteristic advancement in phase at the top surface, which turns into a phase lag at depths of approx. 2 mm and greater. The positive phase shift at the surface was demonstrated experimentally in a previous study [17].
- The spatial decay of the time-maximum of the magnetic induction is consistent with the standard skin-depth formula. This suggests, that this simple and practical formula can be reliably used in the initial prediction of magnetic field inside a DCBN set-up.
- The AMA is acceptably close to the expected NMA provided that the set-up operates within a linear portion of the B(H) material characteristics. Otherwise there is a non-negligible dependency of all the studied magnetisation parameters on NMA. This effect is accounted for by the uneven saturation of both C-Cores. As expected, the maximum induction generated in the plate for a constant, high current magnitude, is higher at 45° than at 0°/90°.
- When comparing the low-current and high-current source magnitudes, the resulting magnetisation patterns have been shown to differ significantly, both quantitatively and qualitatively.

From a practical point of view, the presented simulations allow determination of an optimum workpoint of DCBN set-

up, at which the magnetic induction in the plate is as high as possible without introducing uncontrollable distortions due to B(H) saturation.

Transforming the calculated B(x,y,z,t) function into numerical local MBN patterns, and comparing them against experimental results, is a pending task.

Acknowledgments This study was partly funded by Polish National Centre for Research and Development (Grant MAGSTRESS Number PBS1/A9/14/2012).

Conflict of interest The authors declare that they have no conflict of interest.

References

1. Shah, V.N., MacDonald, P.E.: Residual Life Assessment of Major Light Water Reactor Components, p. 144. Idaho National Engineering Laboratory, Seattle (1987)
2. Jiles, D.C.: The effect of stress on magnetic Barkhausen activity in ferromagnetic steels. NDT E Int. **29**(5), 343 (1996)
3. Augustyniak, B., Degauque, J.: Magneto-mechanical properties evolution of Fe-C alloy during precipitation process. Mater. Sci. Eng. A **370**(1–2), 376–380 (2004)
4. Kwun, H.: Investigation of the dependence of Barkhausen noise on stress and the angle between the stress and magnetization directions. J. Magn. Magn. Mater. **49**(3), 235–240 (1985)
5. Sablik, M.J., Augustyniak, B., Chmielewski, M.: Modeling biaxial stress effects on magnetic hysteresis in steel with the field and stress axes noncoaxial. J. Appl. Phys. **85**(8), 4391–4393 (1999)
6. Buttle, D.J., Dalzell, W., Scruby, C.B., Langman, R.A.: Comparison of three magnetic techniques for biaxial stress measurement. NDT E Int. **29**(5), 342 (1996)
7. Mandache, C., Krause, T.W., Clapham, L.: Investigation of optimum field amplitude for stress dependence of magnetic Barkhausen noise. IEEE Trans. Magn. **43**(11), 3976–3983 (2007)
8. Stefanita, C.G.: From Bulk to Nano—The Many Sides of Magnetism, Ch.2. Barkhausen Noise as a Magnetic Nondestructive Testing Technique. Springer, New Jerssey 2008. ISBN: 978-3-540-70547-5
9. Lindgren, M., Lepistö, T.: On the stress vs. Barkhausen noise relation in a duplex stainless steel. NDT E Int. **37**(5), 403–410 (2004)
10. Augustyniak, B., Piotrowski, L., Augustyniak, M., Chmielewski, M., Sablik, M.J.: Impact of eddy currents on Barkhausen and magnetoacoustic emission intensity in a steel plate magnetized by a C-core electromagnet. J. Magn. Magn. Mater. **272**, E543–E545 (2004)
11. Augustyniak, M., Augustyniak, B., Chmielewski, M., Sadowski, W.: Numerical evaluation of spatial time-varying magnetisation of ferritic tubes excited with a C-core magnet. J. Magn. Magn. Mater. **320**, e1053–e1056 (2008)
12. Vengrinovich, V., Tsukerman, V.: Stress and texture measurement using Barkhausen noise and angular scanning of driving magnetic field. In: Conf. Proceedings of 16th WCNDT 2004 World Conference on NDT, Montreal, 2004
13. Zurek, S., Marketos, P., Meydan, T., Moses, A.: Use of novel adaptive digital feedback for magnetic measurements under controlled magnetizing conditions. IEEE Trans. Magn. **41**(11), 4242–4249 (2005)
14. Pólik, Z., Kuczmann, M.: Measuring and control the hysteresis loop by using analog and digital integrators. J. Optoelectron. Adv. Mater. **10**(7), 1861–1865 (2008)
15. White, S., Clapham, L., Krause, T.W.: A multi-channel magnetic flux controller for periodic magnetizing conditions. IEEE Trans. Instr. Meas. **61**(7), 1896–1907 (2012)
16. Augustyniak, M.: Analysis of magnetisation distribution in NDT of ferromagnetic materials. Ph.D. Thesis, Gdansk University of Technology 2007
17. Augustyniak, M., Augustyniak, B., Sablik, M., Sadowski, W.: The finite element method (FEM) simulation of the space and time distribution and frequency dependence of the magnetic field, and MAE. IEEE Trans. Magn. **43**(6), (2007)